

Strong dependency of the tribological behavior of CuZr-based bulk metallic glasses on relative humidity in ambient air

Solène BARLEMONT¹, Paul LAFFONT², Rémi DAUDIN², Alexis LENAIN³, Guillaume COLAS¹, Pierre-Henri CORNUAULT^{1,*}

¹ Femto-ST Institute, Department of Applied Mechanics, University of Bourgogne Franche-Comté, CNRS/UFC/ENSMM/UTBM, Besançon 25030, France

² University of Grenoble Alpes, CNRS, SIMaP, Grenoble 38000, France

³ Vulkam Inc. Amorphous metal micro casting, Gières 38610, France

Received: 28 February 2022 / Revised: 05 July 2022 / Accepted: 03 August 2022

© The author(s) 2022.

Abstract: Thanks to their outstanding mechanical properties, Bulk Metallic Glasses (BMGs) are new alternatives to traditional crystalline metals for mechanical and micromechanical applications including power transmission. However, the tribological properties of BMGs are still poorly understood, mostly because their amorphous nature induces counter intuitive responses to friction and wear. In the present study, four different BMGs ($\text{Cu}_{47}\text{Zr}_{46}\text{Al}_7$, $\text{Zr}_{46}\text{Cu}_{45}\text{Al}_7\text{Nb}_2$, $\text{Zr}_{60}\text{Cu}_{28}\text{Al}_{12}$, and $\text{Zr}_{61}\text{Cu}_{25}\text{Al}_{12}\text{Ti}_2$) underwent ball-on-disc friction tests against 100Cr6 steel balls (American Iron and Steel Institute (AISI) 52100) at different relative humidities (RHs) ranging from 20% to 80%. Controlling humidity enabled to observe a high repeatability of the friction and wear responses of the BMG. Interestingly, the friction coefficient decreased by a factor of 2 when the humidity was increased, and the wear rate of BMGs was particularly low thanks to a 3rd-body tribolayer that forms on the BMG surface, composed of oxidized wear particles originating from the ball. The morphology of this tribolayer is highly correlated to humidity. The study also identifies how the tribolayer is built up from the initial contact until the steady state is achieved.

Keywords: Bulk Metallic Glasses (BMGs); tribology; oxide transfer layer; relative humidity (RH)

1 Introduction

Bulk Metallic Glasses (BMGs) are known for their particularly favorable mechanical properties, among which is a combination of very high yield strength with high elastic strain [1]. Some BMGs also exhibit very high corrosion resistance and biocompatibility. For these reasons, BMGs are currently finding novel applications in different fields including sporting goods, medical implants, defense and space applications, and micromechanical systems (micro harmonic drive and microgears) [2–6]. The final category requires a good surface finish and durable tribological properties, i.e., good friction and wear properties.

However, the tribological behavior of BMGs remains poorly understood, and the literatures tend to demonstrate that they exhibit unpredictable wear resistance. Among the few studies on the tribological behavior of BMGs, the results and interpretations are conflicting, which leads to poor understanding regarding their performances. Nonetheless, the studies show that many typical tribological factors do not explicitly impact or determine the friction and wear properties of BMGs: contact conditions (normal load and sliding velocity) [7–10], relaxation and partial crystallization, which improves or worsens wear resistance [11–17], or mechanical properties of BMGs (e.g., hardness which is not correlated with wear

* Corresponding author: Pierre-Henri CORNUAULT, E-mail: pierre-henri.cornuault@ens2m.fr

resistance) [7, 11, 18–21]. Contrary to most materials, BMGs do not seem to follow Archard's law [22], which predicts a linear relationship between hardness and wear volume of a material. Nonetheless, many authors still try to make a connection between BMG wear resistance and their mechanical properties (hardness [18], toughness [6, 20], and bulk modulus [21]), but no common agreement emerges. The difficulty to explain the observed tribological behavior may find its root in the distinctive plastic strain of BMGs, described as homogenous flow at high temperatures (near or above the glass transition temperature (T_g)) and shear band-mediated plastic deformation at lower temperatures [3, 4]. This may indeed lead to completely different wear mechanisms, as compared to their crystalline counterparts. Instead of work-hardening for crystalline structures, several authors [10, 15, 23, 24] highlight a work-softening behavior of BMGs, leading to surface softening after friction. Jiang et al. [11] pointed to a connection between hardness, free volumes, and crack propagation, in order to explain this work-softening typical behavior of BMGs. The tribological consequences result in subsurface softening after friction, because of the creation of shear bands and free volumes [15].

Among BMGs, CuZr-based BMGs are known for the advantageous combination of the high glass forming ability (GFA) of Zr-based BMGs [3, 25], with the good mechanical properties of Cu-based BMGs, especially their ductility and strength [25]. CuZr-based BMGs already demonstrate a proven interest in microgears [6], but there is little detailed understanding of their friction and wear mechanisms. Salehan et al. [27] suggested a classification of wear mechanisms of Zr-based BMGs into three categories: (1) microcracks followed by delamination and abrasive wear by detached particles, (2) shear banding and subsequent work-softening, and (3) oxide tribolayer formation and possible peeling-off. The third category introduces a possible contribution of oxide tribolayer in the friction and wear behavior of BMGs, in addition to the mechanical contribution discussed above. Indeed BMGs are known for their higher sensitivity to oxidation than their crystalline counterparts [11, 14, 28], and a few studies based on the atomic force microscopy (AFM) measurements deal with the tribological

impact of the native oxide present on the surface of BMGs [29–31]. At the macroscale, some tribological studies highlight the formation of an oxide tribolayer that forms during friction [10, 11, 14, 17, 25]. Such tribolayer formation sometimes results from material transfer [8, 13, 15, 23, 32, 33]. Oxidation highly depends on the oxidative environments considered, and the effective control of relative humidity (RH) is often lacking in tribological studies. RH has been shown to be of great importance, because it can have a strong impact on the tribology of metals and ceramics [34, 35]. In the field of BMGs, very few studies considered the composition of the contact's surrounding environment in the study of friction and wear, but the few that do exclusively focus on vacuum, argon, and oxygen [24, 36, 37]. Wu et al. [36] highlighted a larger wear of Zr-based BMGs in oxygen (6% RH) compared to that in air (40% RH), due to the formation of hard crystalline ZrO_2 particles in oxidative environment. Fu et al. [24] studied the wear rates of Zr-based BMGs in air and vacuum. BMGs suffer from larger wear in air because of oxygen-rich patches that form in the friction track, and which transform into hard and abrasive particles. Jones et al. [37] compared the tribological behavior of Zr-based BMGs in air and low- O_2 environment. The formation of a mixed metal-oxide layer due to the high rate of oxygen in air is responsible of an increase of friction coefficient. While these previous studies investigated the tribological impact of oxygen in air, to the best of our knowledge, there is no study dealing with the impact of RH on the tribological behavior of BMGs. The current work aims to investigate the frictional and wear behavior of the four selected BMGs with controlled RHs.

2 Materials and methods

2.1 Sample preparation

Four BMG compositions have been selected for this study; two compositions have an equivalent ratio of Cu and Zr ($Cu_{47}Zr_{46}Al_7$ and $Cu_{45}Zr_{46}Al_7Nb_2$, at%), named CuZr and CuZr+Nb, respectively; and the other two compositions are rich in Zr ($Zr_{60}Cu_{28}Al_{12}$ and $Zr_{61}Cu_{25}Al_{12}Ti_2$, at%), named Zr and Zr+Ti, respectively.

The BMG samples were produced by arc-melting fragments of each elements of high purity (> 99.9%) under an argon atmosphere. The melting operation was repeated five times to ensure a high chemical homogeneity. The primary alloys obtained were then injected into dedicated molds to produce plate-shaped samples of 15 mm × 10 mm × 1 mm. The X-ray diffraction measurements were performed to ensure the amorphous structure of each composition, using an X-ray diffractometer (X'Pert Pro MPD, PANalytical) with Cu-K α radiations (Fig. S1 in the Electronic Supplementary Material (ESM)). Main mechanical properties of BMG plates are listed in Table 1. The Young's moduli were determined using ultrasonic techniques, and the Vickers hardness was measured under a load of 1 kg during 10 s (means and standard deviations are calculated from 20 measurements within two different samples).

Prior to the friction tests, plates were mechanically polished with sandpaper (until P4000 grade) until a mean S_a close to 70 nm (Table 1). Then, they were ultrasonically cleaned in high-purity isopropyl-alcohol during 3 min at 70 °C before being dried in air. The roughnesses of the polished samples were characterized by variable focus optical microscope (InfiniteFocus, Alicona Imaging GmbH). The mean S_a parameters and associated standard deviations were calculated from three measurements performed on 200 μm × 270 μm areas.

2.2 Friction tests

Friction tests were performed by using an in-house designed ball-on-plate tribometer in dry sliding condition against 5 mm diameter 100Cr6 steel balls (American Iron and Steel Institute (AISI) 52100) of grade 10 quality. 100Cr6 is widely used in tribological

tests [38] and additionally in industrial applications such as ball bearings [39]. The contact conditions chosen for the tests are reciprocating linear motion with a ± 1 mm displacement stroke at 1 Hz, i.e., a sliding speed of 4 mm/s. Test duration ranged from 200 to 10,000 cycles, one cycle being both the back and forth motions. A constant normal force (F_N) of 1 N was applied using dead weight, which corresponds to an initial maximal Hertzian contact pressure of 520 and 540 MPa for Zr-based plates and CuZr-based plates, respectively. A linear variable differential transformer (LVDT) sensor measured the relative displacement of the ball during the tests (Δh). A piezoelectric sensor (9203, KISTLER, Germany) measured the friction force (F_T). For each friction cycle, an average friction coefficient (μ_i) is calculated from an energetic point of view by using Eq. (1), where Δh_0 (= 2 mm) refers to the track length. That also corresponds to the points where $F_T = 0$, namely the extremities of the track, where the motion direction changes. For each test, a stabilized friction coefficient (μ_{stab}) is then calculated by Eq. (2). μ_{stab} corresponds to the mean of all μ_i values of the steady state friction. That means that μ_{stab} is calculated from the cycle, at which the steady state (N_{stab}) begins to the end of the test (cycle N). $\Delta\mu_i$ refers to the standard deviation of μ_i over the same range of cycles.

$$\mu_i = \frac{1}{2\Delta h_0} \int \frac{|F_T|}{F_N} dh \quad (1)$$

$$\mu_{\text{stab}} = \frac{1}{N - N_{\text{stab}}} \sum_{i=N_{\text{stab}}}^N \mu_i \quad (2)$$

To control the RH, the whole tribometer was located in a tightly sealed chamber. An external flask containing solutions of sodium hydroxide (NaOH) with variable concentrations was used to control the

Table 1 Denominations, compositions, and mechanical properties of the studied BMGs. Asterisks refer to the data from Refs. [21, 33].

	Sample denomination	Composition (at%)	Young's modulus (GPa)	Poisson's ratio	Hardness (HV)	Roughness parameter, S_a (nm)
CuZr-based	CuZr	Cu ₄₇ Zr ₄₆ Al ₇	90	0.36*	480±5	68±4
	CuZr+Nb	Cu ₄₅ Zr ₄₆ Al ₇ Nb ₂	90	0.36*	485±5	73±2
Zr-based	Zr	Zr ₆₀ Cu ₂₈ Al ₁₂	83	0.36*	452±4	75±5
	Zr+Ti	Zr ₆₁ Cu ₂₅ Al ₁₂ Ti ₂	83	0.36*	453±4	61±2
	Ball	100Cr6	210*	0.29*	805*	97±5

RH from 20% to 80%, as described in Refs. [40, 41]. Air circulation from the flask to the chamber was ensured by a peristaltic pump. A fan located in the closed chamber allowed to homogenize the RH until reaching the desired value, and was turned off before starting friction tests. RH was continuously monitored throughout the test with an hygrometer (ALMEMO® Control, Ahlborn Mess- und Regelungstechnik GmbH; $\pm 0.1\%$). The standard deviation of RH during a single test was $\pm 1\%$. All friction tests were performed at room temperature (25 ± 2 °C).

2.3 Surface analyses

The surface topography of each friction tracks (plates and balls) was characterized by using a variable focus optical microscope. The raw three-dimensional (3D) surface topography images were processed with the software Gwyddion in order to measure the roughness and to calculate the wear volume, according to the method described by Ayerdi et al. [42]. First, both plate and ball surfaces were flattened by subtracting analytical surfaces obtained from the least-square method corresponding either to the analytic closest plane (for plates) or the quadratic surface (for balls). The wear volumes were then calculated in reference to the resulting mean plane. According to this definition, a positive volume means a loss of matter (e.g., detachment of materials, ploughing grooves, and ejected particles), and a negative volume means an addition of matter (material transfer and pile up). The total wear volume is calculated as the addition of the positive and negative volumes. The wear rates ($\text{mm}^3/(\text{N}\cdot\text{m})$) of the plate (K_p) and the ball (K_b) were defined as the wear volume normalized by units of sliding distance and F_N , as described by Eq. (3), where V_{plate} (mm^3) and V_{ball} (mm^3) are the wear volumes of the plate and the ball, respectively, and $2d$ is the distance covered in one cycle (with $d = 2$ mm in the actual configuration).

$$K_p = \frac{V_{\text{plate}}}{2dN_{\text{cycles}}F_N}$$

$$K_b = \frac{V_{\text{ball}}}{2dN_{\text{cycles}}F_N} \quad (3)$$

All wear tracks were also studied by means of the optical microscope (VHX-7000, Digital Microscope Keyence). In order to estimate the 3rd-body coverage of the wear tracks, images are post-processed with the software ImageJ as per the method described in Fig. S2 in the ESM.

The scanning electron microscopy (SEM) observations were then performed on wear tracks, using a scanning electron microscope (Apreo, FEI) equipped with a secondary electron (SE) detector and a backscattered electron (BSE) detector. The electron beam voltage and current were 5 keV and 0.1 nA, respectively. The energy dispersive spectroscopy (EDS) analyses were conducted at 5 keV with an EDS detector (SD, Bruker). A 3D-SEM image combined with the EDS cartography was achieved by using the software Mountains® (Digital Surf). A focused ion beam (FIB) cross section of the friction track was performed by using a SEM (55 MEG-FEG, Zeiss Ultra) through a regular cross section performed at 30 keV and 2.5 nA followed by two successive cleaning cross sections performed with a beam voltage of 30 keV and lower currents of 0.4 nA and 80 pA, respectively.

The X-ray photoelectron spectroscopy (XPS) analyses were performed on BMG pristine surfaces prior to friction tests (after polishing and cleaning) and after friction tests (in the wear tracks) with an Al-K α monochromatic excitation source. Information about the chemical elements constituting the extreme surface until an approximate depth of 2 nm are thus provided. A semi-quantitative analysis was made possible by the atomic sensitivity factor method [43], whose calculation is based on the area underneath each peak (Table 2).

3 Results

3.1 XPS analyses on raw surfaces

The energy of each peak indicates that all the elements are in oxidized forms, namely ZrO₂, Cu₂O, Nb₂O₅, TiO₂, and different aluminum oxides including Al₂O₃ and Al(OH)₃ (Fig. S3 in the ESM). Among all BMG compositions, the major detected elements are Zr and Al (Table 2). Surprisingly, Cu is present in negligible proportion as compared to the bulk compositions

Table 2 Semi-quantitative analyses by the XPS of the extreme surfaces of the four alloys after polishing and cleaning in isopropanol. Numbers in brackets refer to the theoretical atomic compositions of the bulk materials.

Composition (at%)	Zr		Cu		Al		Nb		Ti		Si
CuZr	55.7	(46)	9.5	(47)	24.9	(7)	—	—	—	—	9.9
CuZr+Nb	46.7	(46)	12.3	(45)	27.8	(7)	2.4	(2)	—	—	10.8
Zr	63.3	(60)	1.7	(28)	24.3	(12)	—	—	—	—	10.6
Zr+Ti	62.1	(61)	1.6	(25)	22.0	(12)	—	—	2.1	(2)	12.3

(Table 1). In comparison, Zr-based (both Zr and Zr+Ti) contain more than 60 at% of Zr and less than 2 at% of Cu. CuZr-based (both CuZr and CuZr+Nb) contain less Zr (approx. 50 at%) and more Cu (approx. 10 at%). Regarding Al, its detection ranges from 22 to 30 at% on all surfaces, much more than that in the bulk (7–12 at%). Microalloying metals, Ti (in Zr+Ti) and Nb (in CuZr+Nb), are detected in the same proportion as that in the bulk (2 at%). It is assumed that the presence of Si may come from the polishing process.

The results are in good agreement with Ref. [30], revealing that a thin oxide film of a few nanometers grows on the surface of most BMGs exposed to ambient conditions. Regarding CuZr-based BMGs, several authors [43–45] show that after annealing, surfaces are enriched in Zr and Al, while the Cu content drops significantly. Most identified oxides are ZrO_2 , Al_2O_3 , and Cu_2O [43, 46]. Kilo et al. [45] describes a Cu and Zr dissociation mechanism during oxidation, leading to a bilayer surface with a Zr-rich layer on the top surface and a Cu-rich layer underneath. This might be explained by the fact that the formation of ZrO_2 and Al_2O_3 is thermodynamically more favorable than that of the Cu_2O oxide [43].

3.2 Tribological test repeatability

A first set of tribological tests was conducted to identify whether the friction behavior of BMGs is repeatable or not in similar conditions of RH, F_N , and sliding speed. Four tests were carried out at 50%±1% RH, 1 N, and during 5,000 cycles. The variation of the friction coefficient for each BMG is displayed in Fig. 1(a). The variation of the friction coefficient is highly similar between the four tests for each BMG. The running-in process occurring during the first 2,000 cycles is identical between Zr-based (both Zr

and Zr+Ti) and between CuZr-based (both CuZr and CuZr+Nb) BMGs. It is however slightly different between the two BMG categories. The steady-state regime of friction is quickly reached: from 2,000 cycles, μ_i is considered as stable for all tests. μ_{stab} defined in Eq. (2) is therefore calculated by $N_{stab} = \frac{2}{5} N$. That means that μ_{stab} calculated for a test of 5,000 cycles is the mean of all μ_i calculated for each cycle between 2,000 and 5,000 cycles (Fig. 1(a)).

The values of μ_{stab} are equal to 0.70 ± 0.02 , 0.67 ± 0.03 , 0.69 ± 0.04 , and 0.67 ± 0.03 for CuZr, CuZr+Nb, Zr, and Zr+Ti, respectively. As far as the RH is kept constant, both the running-in process and μ_{stab} are close enough among identical tests to consider a good repeatability of the tests. Only one test was therefore performed for each parameter combination in the following experiments.

3.3 Tribological tests: RH impact

3.3.1 Friction and wear

The μ_i and K_p and K_b as a function of RH are displayed in Figs. 1(b) and 1(c), respectively. A strong dependence of the friction coefficient to RH is highlighted: Starting at 0.95 below 30% RH, the friction coefficient quickly decreases with increasing RH to 0.55 at 80% RH. This variation is similar to whatever the chemical composition of the alloy. Regarding the wear rates, BMG plates show a high wear resistance with wear rates ranging from -2×10^{-5} to 5×10^{-5} $mm^3/(N\cdot m)$. Most of the values stay close to zero, and some are even negative, meaning that material transfer from the ball to the plate occurred. This is consistent with K_b , which are up to 10 times larger than K_p . K_b strongly depends on RH: K_b decreases when RH increases.

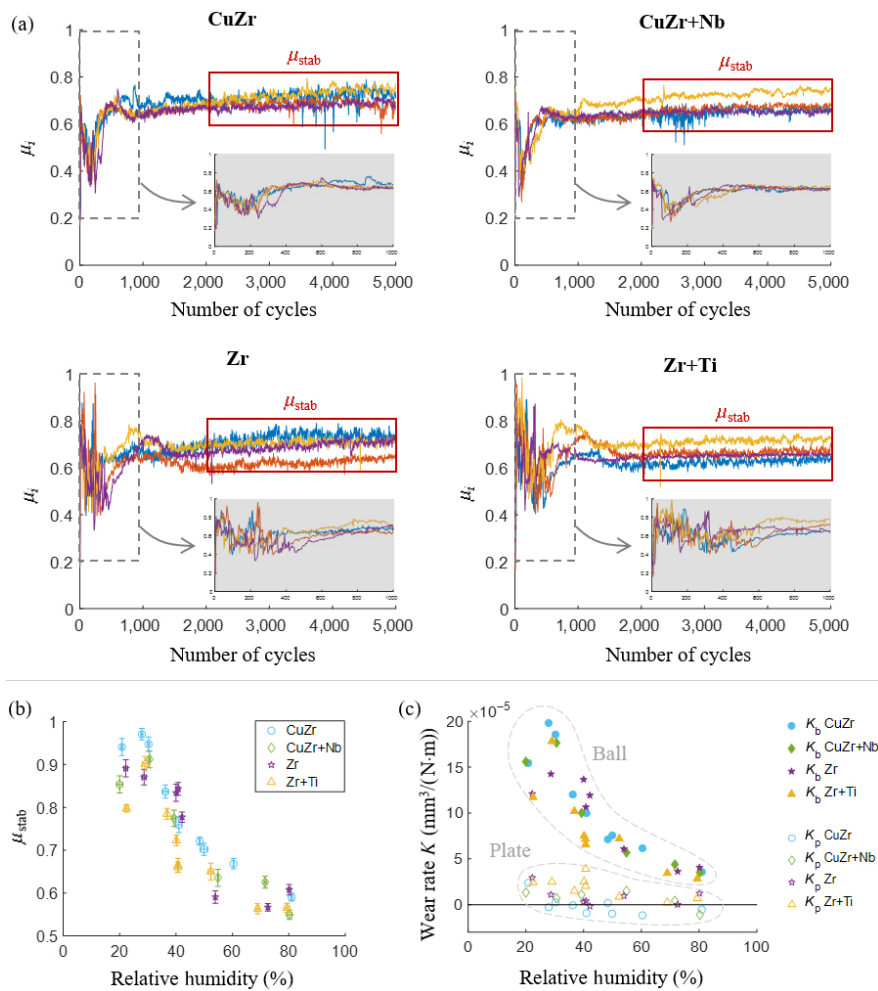


Fig. 1 (a) Repeatability tests performed on the four BMG compositions, μ_i is against the number of cycles, RH = 50%±1%, and $F_N = 1$ N. (b) μ_{stab} vs. RH with standard deviation bars associated to $\Delta\mu_i$ (in ordinate) and ΔRH (in abscissa). (c) K_p (unfilled markers) and K_b (filled markers) vs. RH.

3.3.2 Morphologies and compositions of wear tracks

Figure 2(a) displays optical images of Zr+Ti wear tracks after friction tests performed at 80% and 20% RHs. Observations emphasize the presence of a 3rd-body at the contact interface. At 80% RH, the wear track on the plate is thin and covered with expanded and smooth patches that lay on the surface, and large amounts of small particles are also distributed around the patches (Fig. 2(c)). At 20% RH, the wear track is larger and covered with small rough patches that are homogeneously distributed over the track. Two profiles extracted from those tracks (Fig. 2(b)) show that at 80% RH, the expanded and smooth patches are above the mean surface height; while the island-shaped patches observed at 20% RH are above but below the

mean surface height. Conversely, the wear tracks of all the balls have the shape of a regular disc, without any 3rd-body on the surface (Fig. S4 in the ESM). Wear particles are present outside of the track.

The SEM observations with a BSE detector allowed the identification of two types of 3rd-body patches: Most of the track is covered by dark patches, but a few white patches can be found in some localized areas (Fig. S5 in the ESM). The BSE detector enables the differentiation of the light elements (i.e., low atomic number (Z)) and the heavy elements (i.e., high Z), leading to a grey scale correlated to the elemental composition, where the heavy elements appear brighter than the light ones. The EDS analysis revealed that the dark patches are mostly composed of Fe and O, while the light patches are composed of Cu, Zr, Al,

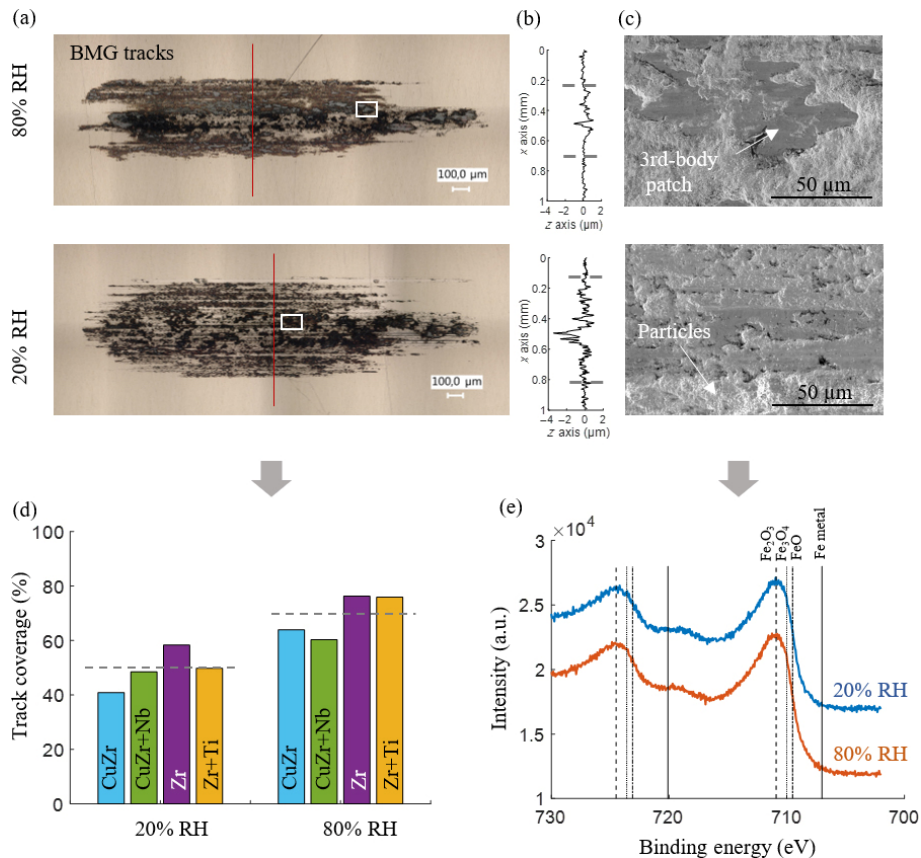


Fig. 2 (a) Optical images of Zr+Ti wear tracks after friction tests at 80% RH and 20% RH. (b) Height profiles along the red lines at 80% RH and 20% RH. The dashed lines represent the boundaries of the wear tracks. (c) SEM images (SE detector) of the white-framed zones at 80% RH and 20% RH. (d) 3rd-body coverage over the wear tracks at 20%RH and 80% RH for each BMG. The dashed lines represent the average coverages at 20%RH and 80% RH. (e) Fe 2p peaks from the XPS analyses performed on CuZr wear tracks after friction tests at 20% RH (blue) and 80% RH (red). The solid lines refer to the theoretical peaks of Fe metal, dash-dotted lines refer to FeO, dashed lines refer to Fe₂O₃, and dotted lines refer to Fe₃O₄ [47].

and O (Fig. S5(c) in the ESM). This suggests that most of the 3rd-body patches come from the oxidized wear debris of the ball (Fe-oxides), and only a few patches come from the oxidized wear debris of the BMG (Zr–Cu–Al-oxides). Two different structures of 3rd-body patches are observed: Either the superposition of Fe-oxides that spread over Zr–Cu–Al-oxides (Fig. S5 in the ESM) or a succession of Zr–Cu–Al-oxides and Fe-oxide layers lead to a mixed dark–white patch in zebra stripes perpendicular to the sliding direction (Fig. 3(b) and Fig. S6 in the ESM). The latter extend beneath the surface until a depth superior to 1 μm , as shown by the FIB cross section displayed in Fig. 3(c). Their morphologies suggest a very high plastic deformation and surface ductility of the 3rd-body. There are porosities at the root of some stripes, and the greyscale contrast along the stripes exhibits

a complex composite structure of Fe-oxides and Zr–Cu–Al-oxides (Fig. 3(d)).

However, there are only few Zr–Cu–Al-oxide patches, and most of the 3rd-body layer is composed of dark-appearing Fe-oxide patches. The XPS analyses performed over the friction tracks of CuZr samples after tests at 20% and 80% RHs are displayed in Fig. 2(e). The Fe 2p_{3/2} peak positions at 20% and 80% RHs are 710.8 and 710.9 eV, respectively. This corresponds to Fe₂O₃ oxides according to the theoretical binding energy of Fe₂O₃ 2p_{3/2} peak, which is located at 710.9 eV [47]. This shows that the nature of iron oxide formed and consequently of the dark patches remain the same from 20% to 80% RHs.

Using the BSE detector, it becomes easy to differentiate the dark 3rd-body layer from the BMG raw surface. The strong proportion of Fe-oxides constituting

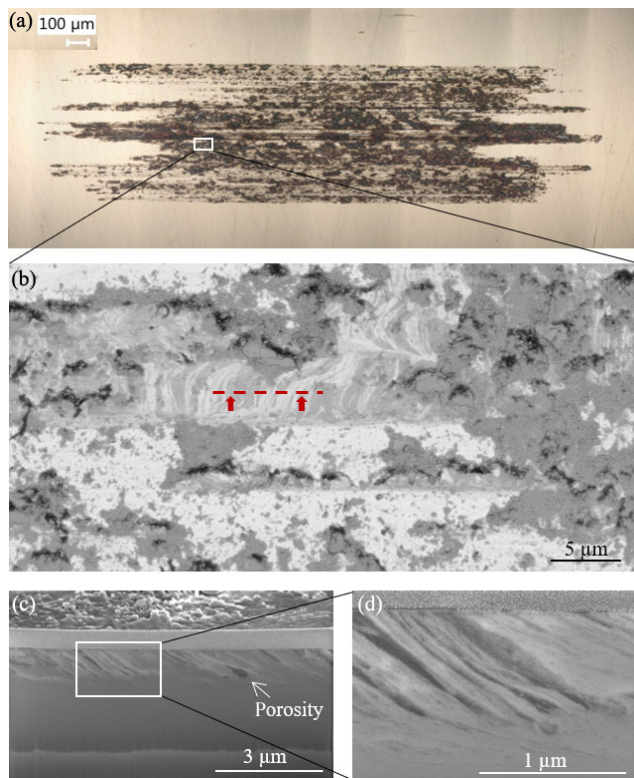


Fig. 3 (a) Optical image of a CuZr+Nb wear track at 20% RH and (b) MEB observation (BSE) associated to the white-framed zone. (c, d) FIB cross section performed along the red dashed line.

the 3rd-body is indeed responsible for a sharp grey-level contrast (Fig. S2 in the ESM). Using image binarization of the related images, the 3rd-body coverage is estimated around 49% on average for the track at 20% RH and around 69% on average for the track at 80% RH (Fig. 2(d)). That demonstrates that the higher the humidity, the larger the coverage. Note that the coverage ratio was calculated on the whole central part of the wear track deprived of its extremities.

The combination of the XPS analyses and wear track coverage shows that humidity only affects the track coverage and morphology of the 3rd-body, but not its chemical nature (Figs. 2(c)–2(e)).

3.4 Tribological tests: Increasing number of cycles

3.4.1 Friction and wear

In order to understand the wear mechanism of CuZr-based BMG and more specifically the 3rd-body-formation scenario, a tribological study with increasing number of cycles was performed. Due to high repeatability of the tests (Section 3.2), one test was performed with each following N : 200–350–500–750–1,000–1,500–2,000–3,500–5,000–10,000. The μ_i superposition between each test is displayed in Fig. S7 in the ESM. The RH chosen for this study was 50% RH for three reasons: (1) The nature of the 3rd-body does not change with varying RH, (2) 50% RH corresponds to a medium humidity in ambient conditions, and (3) the stabilization of RH is easier and faster to obtain. Two BMG compositions were selected, namely Zr and CuZr, because of the close tribological behavior exhibited by CuZr and CuZr+Nb on the one hand, and by Zr and Zr+Ti on the other hand (Fig. 1(a)). The μ_{stab} , K_b , and K_p as a function of number of friction cycle are displayed in Fig. 4.

Three successive stages of sliding are highlighted, as shown in the surrounded numbers in Fig. 4:

1) A first stage of sliding is characterized by a large wear rate of the BMG plate and a K_b close to zero. This stage is of different duration between Zr and CuZr: from sliding initiation to 1,000 and 500 friction cycles, respectively.

2) During the second stage, the ball wear rate

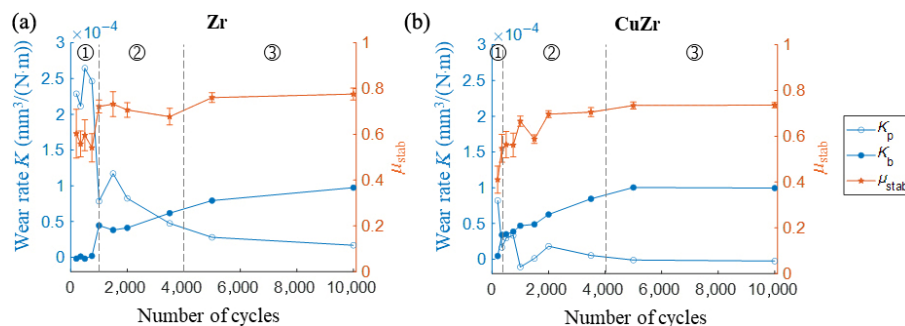


Fig. 4 μ_{stab} (red stars), K_p (unfilled circles), and K_b (filled circles) vs. number of friction cycles. Each point refers to a single test. The standard deviation bars are associated to $\Delta\mu_i$. Tests were performed at $50\% \pm 1\%$ RH for both (a) Zr plate and (b) CuZr plate.

suddenly increases contrary to the BMG wear that decreases until a reversal. The mentioned that reversal occurs at approx. 3,000 cycles and 750 cycles for Zr and CuZr, respectively. The standard deviation of μ_{stab} decreases progressively while μ_{stab} is reaching a stable value.

3) From 4,000 to 10,000 friction cycles, a stabilized value is reached for μ_{stab} , K_p , and K_b . The standard deviation of μ_{stab} reaches a very low value.

3.4.2 Morphologies of wear tracks

The SEM observations carried out on the wear tracks are displayed in Fig. 5. The track becomes larger as the number of cycle increases. First, a ploughing striation is created in the middle of the track, followed by the appearance of other secondary striations when the number of cycle increases. At the extremities of the track and inside of each striation, white 3rd-body patches composed of Zr–Cu–Al-oxides are formed (Fig. S8(a) in the ESM). Beside and among these striations, several dark 3rd-body patches are formed by agglomeration of small wear debris mainly composed of iron oxides, as shown by the BSE images. After more than 4,000 cycles, most of the central part of the track is covered by these dark 3rd-body patches, and no white patches are seen. At each extremity of the track, only one white patch is still visible, positioned in the middle of the facing contact area of the ball (Fig. S8(c) in the ESM).

4 Discussion

In the literature, most oxide tribolayers formed on BMGs are composed of the elements constituting the BMG. Jiang et al. [11], Aditya et al. [17], and Wu et al. [25] studied the tribological behavior of ZrCu-based BMGs ($\text{Zr}_{52.5}\text{Cu}_{17.9}\text{Ni}_{14.6}\text{Al}_{10}\text{Ti}_5$, $\text{Zr}_{57}\text{Cu}_{15.4}\text{Ni}_{12.6}\text{Al}_{10}\text{Nb}_5$, and $(\text{Cu}_{50}\text{Zr}_{50})_{97-x}\text{Al}_x\text{Y}_3$, respectively) under ball-on-plate reciprocating sliding against 100Cr6, WC, and Si_3N_4 counterparts, respectively. Wang et al. [10] studied a $(\text{Zr,Cu})_{95}\text{Al}_5$ BMG under pin-on-disk configuration against a GCr6 steel counterpart. All these works describe a tribolayer adhering to the BMG surface composed of oxidized elements of the BMG. For instance, Jiang et al. [11] observed the formation of an oxide-based layer when testing $\text{Zr}_{52.5}\text{Cu}_{17.9}\text{Ni}_{14.6}\text{Al}_{10}\text{Ti}_5$ against 100Cr6. Wear scars were described into two distinct regions: abrasion regions and adhesion regions covered by dark patches. Contrary to the present work, dark patches were exclusively composed of oxidized elements of the BMG, and no iron oxides were detected. A similar BMG sample was thermally and mechanically treated until a crystalline state, and no oxide layer was observed after friction tests. Oxidative wear is thus believed to be one of the predominant wear mechanisms of amorphous metallic alloys. On the other hand, Zhao et al. [13], Wu et al. [15], and Wu et al. [23] described a material transfer from the BMG to the counterface by adhesive wear,

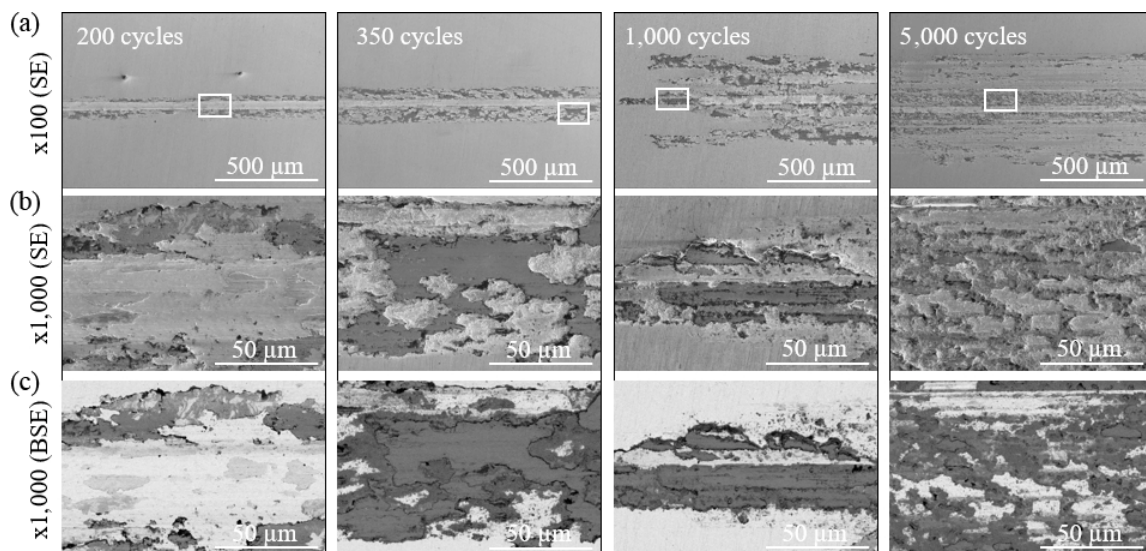


Fig. 5 (a) SEM observations of wear tracks on the CuZr plate after 200, 350, 1,000, and 5,000 friction cycles at 50% RH (SE detector). (b and c) Images correspond to a 10-time higher magnification of the white-framed areas, with both SE and BSE detectors.

under pin-on-disk friction tests among ZrCu-based BMGs ($Zr_{61}Ti_2Cu_{25}Al_{12}$, $Zr_{41.2}Ti_{13.8}Cu_{12.5}Ni_{10}Be_{22.5}$, and $Zr_{52.5}Cu_{17.9}Ni_{14.6}Ti_5Al_{10}$, respectively) against steel (unspecified), bearing steel, and stainless steel, respectively. In all of these situations, BMGs experience a severe wear through particle generation and the formation of a tribolayer composed of the BMG elements. More rarely, material transfer from the counterface to the BMG surface occurs, but only in specific cases such as that (1) the counterface is softer than the BMG surface [19], (2) material transfer concerns only the carbon present in the counterface that mixes with BMG oxides [8], and (3) material transfer of Fe occurs when Fe is already present in the BMG composition [32, 48]. To the best of our knowledge, only one study deals with the formation of a similar tribolayer, as observed in the present study composed of the particles of the harder steel counterpart, which form a protective layer over the BMG surface. Indeed, Cornuault et al. [33] observed a comparable tribolayer when testing $Zr_{52.5}Cu_{17.9}Ni_{14.6}Al_{10}Ti_5$ against 100Cr6 with similar contact conditions (reciprocating sliding at 4 mm/s, during 10,000 cycles of ± 1 mm, in ambient air, and at 680 MPa of initial maximal Hertzian contact pressure).

Figure 1(b) highlights the strong dependence of RH during friction of the couple CuZr-based BMGs/100Cr6. This impact of RH is significant on the morphologies of patches and 3rd-body coverage of the BMG tracks, where they become larger with increasing RHs. However, this morphological change is not supported by a chemical change of the oxides formed, which remain Fe_2O_3 regardless of the RH (Fig. 2(e)). This means that RH does not affect the chemical nature of the oxide particles, but it rather affects the agglomeration of steel ball debris into 3rd-body patches. According to Leheup and Pendlebury [49], a higher RH would act as an inhibitor for surface oxidation despite the common thought that presupposes an increase of oxidation in wet environment. Indeed, the oxidative process (induced by O_2 presence) is slowed down because of the presence of other molecules in the surrounding atmosphere (H_2O). This phenomenon should lead to an increase of friction coefficient, in opposition to the present results. De Baets et al. [50] observed the same dependency of RH

between two steels: bearing steel ball (C: 1.03%, Si: 0.25%, Mn: 0.35%, and Cr: 1.4%) and cold-down steel (C: 0.11%, Si: 0.03%, Mn: 0.66%, P: 0.047%, S: 0.037%, and Al: 0.023%). Their study highlights a decrease of the friction coefficient from 0.78 at 20% RH to 0.60 at 90% RH. They concluded that the influence of RH was not due to oxidation inhibition, but to boundary lubrication of contacting surfaces. They defined three possible mechanisms to explain this lubricating effect of RH: (1) A change of oxide nature can occur: At low RHs, fretting mainly leads to the formation of Fe_2O_3 that can be inhibited at higher humidities, promoting other types of oxidation reactions. (2) Gas adsorption can occur between a molecule and the metal surface, forming a physisorbed layer that lubricates the contact. (3) Condensation of the moisture can happen at very high RHs, forming a lubricant film. In the present study, both the second and the third mechanisms might be involved, i.e., physisorbed gas molecules and condensed water film between the two surfaces. Moreover, Fe_2O_3 is known to have high capability of water adsorption. Yamamoto et al. [51] demonstrated the increasing molecular adsorption of water on Fe_2O_3 with increasing RHs up to a water coverage superior to 1.5 monolayers. In addition to the lubricant film at the interface, physisorbed water may be present around the wear particles coming from the ball (Fe_2O_3). That might consequently enhance the agglomeration of particles to form the layer patches observed at high RHs.

Regarding the wear scenario leading to the formation of the stable 3rd-body layers and stable friction and wear regimes, tests performed with increasing number of friction cycles allow the identification of three successive stages (Fig. 6).

During the first stage, the hard steel ball creates a first ploughing striation on the softer BMG surface. Wear debris produced during this abrasion process are originating from the native oxide present on the extreme surface. According to the XPS analyses (Fig. S3 in the ESM), they are mainly composed of ZrO_2 , aluminum oxides (Al_2O_3 and $Al(OH)_3$), and Cu_2O . These oxidized particles are compacted and flattened into small patches adhering to the surface of the BMG. The newly exposed surface inside the ploughing striations is probably Cu-enriched according

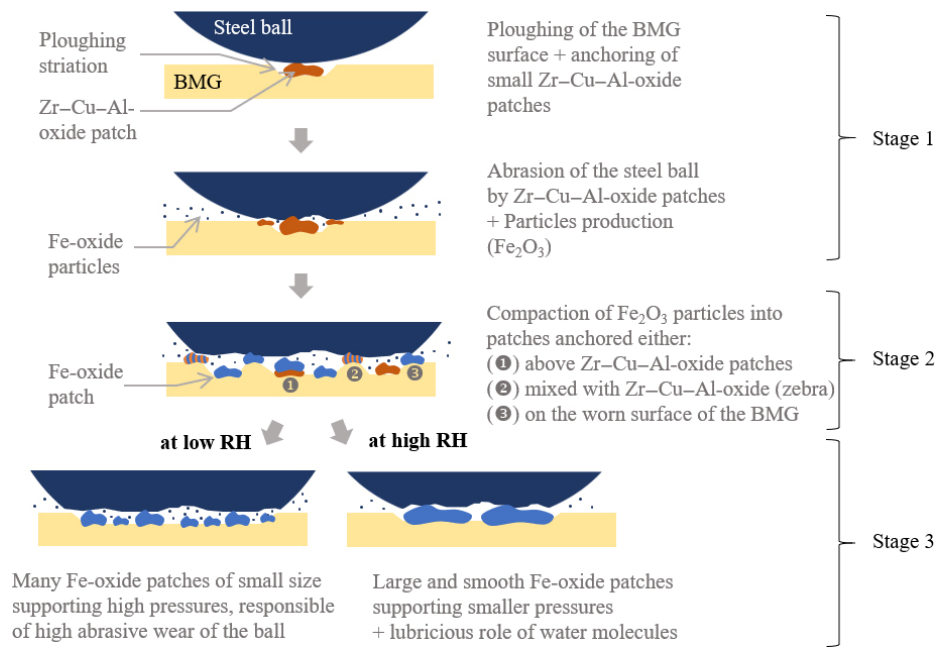


Fig. 6 Scheme of the three successive stages of wear mechanisms involved between CuZr-based plates and 100Cr6 balls.

to the dissociation mechanism described by Kilo et al. [45], with a Cu-rich layer underneath the upper Zr-rich layer. This ploughing mechanism associated to the formation of Zr–Cu–Al-oxide patches can explain the high BMG wear volume and the fluctuating friction coefficient during this early stage of friction. These oxides are known to be hard and abrasive, especially ZrO_2 and Al_2O_3 [52]. Consequently, the abrasive mechanism gradually reverses: The Zr–Cu–Al-oxides become responsible of the progressive abrasion of the steel ball, leading to the production of iron oxide (Fe_2O_3) particles in the contact interface.

During the second stage, Fe_2O_3 particles are compacted into patches and get anchored inside the wear track through three distinct processes: (1) Fe-oxide patches adhere to the previously formed Zr–Cu–Al-oxide patches and cover them entirely or partially. (2) Fe_2O_3 get anchored into some cracks on the surface of Zr–Cu–Al-oxide patches. Indeed, adhesion between steel ball and BMG plate may induce some crack openings, in which iron oxide particles are trapped. Then, the successive forward and backward motions promote strain in elongation and trapping, which eventually results into the observed stripe shape. (3) Fe-oxide patches adhere directly to the worn surface of the BMG. As a common prerequisite to these three adhesive mechanisms,

the prior presence of Zr–Cu–Al-oxide patches is necessary to play an anchoring role of Fe_2O_3 patches. The spontaneous adhesion of Fe_2O_3 particles to the BMG surface could be explained by the chemical affinity between Fe and Zr/Al (heat of mixing Fe–Zr = -25 kJ/mol; Fe–Al = -11 kJ/mol) [32]. The wear mechanism described in this study depends on the chemical reactivity of elements Zr–Cu–Al and Fe.

Finally, the third stage corresponds to a steady-state regime. The tribolayer is, on the one hand, responsible of an increase of the wear of the steel ball because of continuous abrasion of the ball by the oxide particles detached from it. On the other hand, it is responsible for a decrease of the BMG wear, thanks to the protective tribolayer that is being formed from those iron oxide particles. However, this steady state is RH dependent. At low RHs, the wide track is covered by small and rough 3rd-body patches, constituting a highly abrasive surface. The ball undergoes severe wear, and a large amount of iron-oxide particles are produced that subsequently leave the contact area. At high RHs, the high water adsorption on Fe_2O_3 leads to the agglomeration of particles into large and smooth 3rd-body patches. Additionally, a lubricant film of water molecules may also contribute to the smaller friction coefficient and wear rates.

The newly formed interface, after the steady state

establishment, is composed of steel (ball) against iron oxides (plate). This is therefore comparable to steel against steel tribological studies with varying humidities. Klaffke [53] studied the tribological contact between two 100Cr6 specimens through fretting tests, and the friction coefficient follows exactly the same variations as in the present study (Fig. 7). Oh et al. [54] also obtained similar results with carbon steels (1020, 1040, and 1045). The behavior is described as severe wear at low RHs (because of adhesive wear in metal–metal contact) to soft wear at high RHs (because of oxides presence and water adsorption). This shows that the tribological behavior of the tested BMG is strongly correlated to the counterpart material. As mentioned above, the wear mechanism described in this study is firstly due to the formation of ZrO_2 – Cu_2O – Al_2O_3 patches formed from the native oxide present on the BMG surfaces, playing afterwards an anchoring site for Fe_2O_3 particles detached from the ball. These Fe-oxide patches protect the BMG from subsequent wear, although 100Cr6 steel is harder than the BMG.

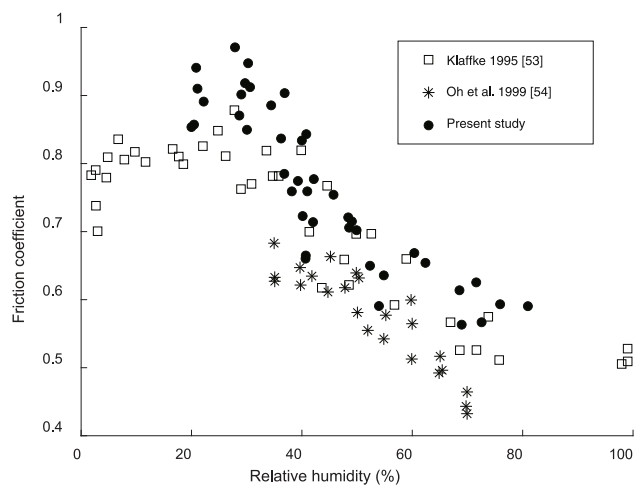


Fig. 7 Friction coefficients depending on RHs of the present study (dots) compared to the results obtained in two different studies: 100Cr6 against 100Cr6 (squares) and carbon steels 1020, 1041, and 1045 against themselves (stars).

5 Conclusions

Until now, the literatures about BMGs tend to exhibit an erratic behavior in their tribological response. This study is a first step towards a reproducibility of the tribological response, as long as the RH is controlled

in addition to the usual contact conditions (F_N , sliding distance, and sliding velocity).

Contrary to crystalline metals, for which hardness is a determinant parameter, the relationship between hardness and the tribological behavior of BMGs is debatable. Indeed, this work highlights a surprising wear resistance of CuZr-based BMGs provided by a 3rd-body tribolayer composed of Fe_2O_3 oxides coming from the 100Cr6 ball. Consequently, the BMG gets a protection despite the higher hardness of the counterpart: The 3rd-body patches accommodate friction and protect the BMG substrate from wear. This anchoring process of Fe_2O_3 patches is made possible through an intermediate formation of Zr–Cu–Al-oxide patches composed of the native oxide of BMGs.

The results show a strong influence of RH on the friction and wear of BMGs and 100Cr6. Indeed, the compaction morphology of iron oxides differs depending on RH. In dry environment, large amounts of debris are ejected from the contact, and few are compacted into small patches that plays a role of hard asperities responsible of severe wear of the hard ball. In wet environment, because of the probable presence of physisorbed water molecules and condensed water film, large amounts of debris gather and compact into large and smooth 3rd-body patches, which can reach 3 μm in thickness.

Contrary to most studies, this study highlights the importance of the chosen counterpart on the tribological behavior of BMGs. In this study, the 100Cr6 counterpart is driving the tribological response after a BMG-dependent running-in period. It might be questioned on whether another steel counterpart would lead to the same behavior or not. This would have to be addressed in future works.

Acknowledgements

This work was supported by the EUR EIPHI Graduate School (ANR-17-EURE-0002). The authors are thankful for the financial support provided by the French National Research Agency (ANR) (ANR-19-CE08-0015). The authors thank Olivier HEINTZ and Anna KRYSTIANIAK (ICB lab at Univ. Bourgogne Franche-Comté, France) for providing

the XPS spectrums, Marina RASCHETTI (Femto-ST Institute, France) for her help in using software Mountains® (Digital Surf), Peter SERLES (the NanoMechanics and Materials Laboratory at University of Toronto, Canada) for English spelling and grammar corrections, and the technology center MIMENTO (Femto-ST Institute, France).

Electronic Supplementary Material: Supplementary material is available in the online version of this article at <https://doi.org/10.1007/s40544-022-0680-z>.

Open Access This article is licensed under a Creative Commons Attribution 4.0 International License, which permits use, sharing, adaptation, distribution and reproduction in any medium or format, as long as you give appropriate credit to the original author(s) and the source, provide a link to the Creative Commons licence, and indicate if changes were made.

The images or other third party material in this article are included in the article's Creative Commons licence, unless indicated otherwise in a credit line to the material. If material is not included in the article's Creative Commons licence and your intended use is not permitted by statutory regulation or exceeds the permitted use, you will need to obtain permission directly from the copyright holder.

To view a copy of this licence, visit <http://creativecommons.org/licenses/by/4.0/>.

References

- [1] Inoue A. Bulk glassy alloys: Historical development and current research. *Engineering* **1**(2): 185–191 (2015)
- [2] Inoue A, Nishiyama N. New bulk metallic glasses for applications as magnetic-sensing, chemical, and structural materials. *MRS Bull* **32**(8): 651–658 (2007)
- [3] Telford M. The case for bulk metallic glass. *Mater Today* **7**(3): 36–43 (2004)
- [4] Greer A L. Metallic glasses... on the threshold. *Mater Today* **12**(1–2): 14–22 (2009)
- [5] Niza M E, Komori M, Nomura T, Yamaji I, Nishiyama N, Ishida M, Shimizu Y. Test rig for micro gear and experimental analysis on the meshing condition and failure characteristics of steel micro involute gear and metallic glass one. *Mech Mach Theory* **45**(12): 1797–1812 (2010)
- [6] Hofmann D C, Andersen L M, Kolodziejska J, Roberts S N, Borgonia J P, Johnson W L, Vecchio K S, Kennett A. Optimizing bulk metallic glasses for robust, highly wear-resistant gears. *Adv Eng Mater* **19**(1): 1600541 (2017)
- [7] Prakash B. Abrasive wear behaviour of Fe, Co and Ni based metallic glasses. *Wear* **258**(1–4): 217–224 (2005)
- [8] Parlar Z, Bakkal M, Shih A J. Sliding tribological characteristics of Zr-based bulk metallic glass. *Intermetallics* **16**(1): 34–41 (2008)
- [9] Zhong H, Chen J, Dai L Y, Yue Y, Zhang Z W, Zhang X Y, Ma M Z, Liu R P. Tribological behaviors of Zr-based bulk metallic glass versus Zr-based bulk metallic glass under relative heavy loads. *Intermetallics* **65**: 88–93 (2015)
- [10] Wang Y, Zhang L, Wang T, Hui X D, Chen W, Feng C F. Effect of sliding velocity on the transition of wear mechanism in (Zr,Cu)₉₅Al₅ bulk metallic glass. *Tribol Int* **101**: 141–151 (2016)
- [11] Jiang F, Qu J, Fan G J, Jiang W H, Qiao D C, Freels M W, Liaw P K, Choo H. Tribological studies of a Zr-based glass-forming alloy with different states. *Adv Eng Mater* **11**(11): 925–931 (2009)
- [12] Bhatt J, Kumar S, Dong C, Murty B S. Tribological behaviour of Cu₆₀Zr₃₀Ti₁₀ bulk metallic glass. *Mater Sci Eng A* **458**(1–2): 290–294 (2007)
- [13] Zhao J, Gao M, Ma M X, Cao X F, He Y Y, Wang W H, Luo J B. Influence of annealing on the tribological properties of Zr-based bulk metallic glass. *J Non-Cryst Solids* **481**: 94–97 (2018)
- [14] Jin H W, Ayer R, Koo J Y, Raghavan R, Ramamurty U. Reciprocating wear mechanisms in a Zr-based bulk metallic glass. *J Mater Res* **22**(2): 264–273 (2007)
- [15] Wu X F, Zhang G A, Wu F F. Wear behaviour of Zr-based *in situ* bulk metallic glass matrix composites. *Bull Mater Sci* **39**(3): 703–709 (2016)
- [16] Yong L, Zhu Y T, Luo X K, Liu Z M. Wear behavior of a Zr-based bulk metallic glass and its composites. *J Alloys Compd* **503**(1): 138–144 (2010)
- [17] Aditya A, Wu H F, Arora H, Mukherjee S. Amorphous metallic alloys: Pathways for enhanced wear and corrosion resistance. *JOM* **69**(11): 2150–2155 (2017)
- [18] Greer A L, Rutherford K L, Hutchings I M. Wear resistance of amorphous alloys and related materials. *Int Mater Rev* **47**(2): 87–112 (2002)
- [19] Fleury E, Lee S M, Ahn H S, Kim W T, Kim D H. Tribological properties of bulk metallic glasses. *Mater Sci Eng A* **375–377**: 276–279 (2004)
- [20] Maddala D R, Hebert R J. Sliding wear behavior of Fe_{50-x}Cr₁₅Mo₁₄C₁₅B₆Er_x (x = 0, 1, 2 at%) bulk metallic glass. *Wear* **294–295**: 246–256 (2012)

- [21] Liao Z L, Hua N B, Chen W Z, Huang Y T, Zhang T. Correlations between the wear resistance and properties of bulk metallic glasses. *Intermetallics* **93**: 290–298 (2018)
- [22] Archard J F. Contact and rubbing of flat surfaces. *J Appl Phys* **24**(8): 981–988 (1953)
- [23] Wu H, Baker I, Liu Y, Wu X L, Munroe P R, Zhang J G. Tribological studies of a Zr-based bulk metallic glass. *Intermetallics* **35**: 25–32 (2013)
- [24] Fu X Y, Kasai T, Falk M L, Rigney D A. Sliding behavior of metallic glass: Part I. Experimental investigations. *Wear* **250**(1–12): 409–419 (2001)
- [25] Wu K, Zheng L J, Zhang H. Research on high-Al Cu–Zr–Al–Y bulk metallic glass and its composites. *J Alloys Compd* **770**: 1029–1037 (2019)
- [26] Andersen L M. Toughness of wear-resistant Cu–Zr-based bulk metallic glasses. Ph.D. Thesis. San Diego (USA): University of California, 2016.
- [27] Salehan R, Shahverdi H R, Miresmaeili R. Effects of annealing on the tribological behavior of Zr₆₀Cu₁₀Al₁₅Ni₁₅ bulk metallic glass. *J Non-Cryst Solids* **517**: 127–136 (2019)
- [28] Kai W, Hsieh H H, Nieh T G, Kawamura Y. Oxidation behavior of a Zr–Cu–Al–Ni amorphous alloy in air at 300–425 °C. *Intermetallics* **10**(11–12): 1265–1270 (2002)
- [29] Ma H R, Bennowitz R. Nanoscale friction and growth of surface oxides on a metallic glass under electrochemical polarization. *Tribol Int* **158**: 106925 (2021)
- [30] Kang S J, Rittgen K T, Kwan S G, Park H W, Bennowitz R, Caron A. Importance of surface oxide for the tribology of a Zr-based metallic glass. *Friction* **5**(1): 115–122 (2017)
- [31] Caron A, Sharma P, Shluger A, Fecht H J, Louzguine-Louzguin D V, Inoue A. Effect of surface oxidation on the nm-scale wear behavior of a metallic glass. *J Appl Phys* **109**(8): 083515 (2011)
- [32] Zhou Q, Han W C, Luo D W, Du Y, Xie J Y, Wang X Z, Zou Q G, Zhao X X, Wang H F, Beake B D. Mechanical and tribological properties of Zr–Cu–Ni–Al bulk metallic glasses with dual-phase structure. *Wear* **474–475**: 203880 (2021)
- [33] Cornuault P H, Colas G, Lenain A, Daudin R, Gravier S. On the diversity of accommodation mechanisms in the tribology of Bulk Metallic Glasses. *Tribol Int* **141**: 105957 (2020)
- [34] Lancaster J K. A review of the influence of environmental humidity and water on friction, lubrication and wear. *Tribol Int* **23**(6): 371–389 (1990)
- [35] Chen Z, He X, Xiao C, Kim S H. Effect of humidity on friction and wear—A critical review. *Lubricants* **6**(3): 74 (2018)
- [36] Wu H, Baker I, Liu Y, Wu X L, Munroe P R. Effects of environment on the sliding tribological behaviors of Zr-based bulk metallic glass. *Intermetallics* **25**: 115–125 (2012)
- [37] Jones M R, Kustas A B, Lu P, Chandross M, Argibay N. Environment-dependent tribological properties of bulk metallic glasses. *Tribol Lett* **68**(4): 123 (2020)
- [38] Czichos H, Becker S, Lexow J. Multilaboratory tribotesting: Results from the Versailles Advanced Materials and Standards programme on wear test methods. *Wear* **114**(1): 109–130 (1987)
- [39] Romanowicz P J, Szybiński B. Fatigue life assessment of rolling bearings made from AISI 52100 bearing steel. *Materials* **12**(3): 371 (2019)
- [40] Madge D S. The control of relative humidity with aqueous solutions of sodium hydroxide. *Entomol Exp Appl* **4**(2): 143–147 (1961)
- [41] Stokes R H, Robinson R A. Standard solutions for humidity control at 25 °C. *Ind Eng Chem* **41**(9): 2013 (1949)
- [42] Ayerdi J J, Aginagalde A, Llavori I, Bonse J, Spaltmann D, Zabala A. Ball-on-flat linear reciprocating tests: Critical assessment of wear volume determination methods and suggested improvements for ASTM D7755 standard. *Wear* **470–471**: 203620 (2021)
- [43] Tam C Y, Shek C H, Wang W H. Oxidation behaviour of a Cu–Zr–Al bulk metallic glass. *Rev Adv Mater Sci* **18**(2): 107–111 (2008)
- [44] Nie X P, Yang X H, Chen L Y, Yeap K B, Zeng K Y, Li D, Pan J S, Wang X D, Cao Q P, Ding S Q, et al. The effect of oxidation on the corrosion resistance and mechanical properties of a Zr-based metallic glass. *Corros Sci* **53**(11): 3557–3565 (2011)
- [45] Kilo M, Hund M, Sauer G, Baiker A, Wokaun A. Reaction induced surface segregation in amorphous CuZr, NiZr and PdZr alloys—An XPS and SIMS depth profiling study. *J Alloys Compd* **236**(1–2): 137–150 (1996)
- [46] Kimura H M, Asami K, Inoue A, Masumoto T. The oxidation of amorphous Zr-base binary alloys in air. *Corros Sci* **35**(5–8): 909–915 (1993)
- [47] Hawn D D, DeKoven B M. Deconvolution as a correction for photoelectron inelastic energy losses in the core level XPS spectra of iron oxides. *Surf Interface Anal* **10**(2–3): 63–74 (1987)
- [48] Prakash B, Hiratsuka K. Sliding wear behaviour of some Fe-, Co- and Ni-based metallic glasses during rubbing against bearing steel. *Tribol Lett* **8**(2–3): 153–160 (2000)
- [49] Leheup E R, Pendlebury R E. Unlubricated reciprocating wear of stainless steel with an interfacial air flow. *Wear* **142**(2): 351–372 (1991)

- [50] De Baets P, Kalacska G, Strijckmans K, van de Velde F, van Peteghem A P. Experimental study by means of thin layer activation of the humidity influence on the fretting wear of steel surfaces. *Wear* **216**(2): 131–137 (1998)
- [51] Yamamoto S, Kendelewicz T, Newberg J T, Ketteler G, Starr D E, Mysak E R, Andersson K J, Ogasawara H, Bluhm H, Salmeron M, et al. Water adsorption on α -Fe₂O₃(0001) at near ambient conditions. *J Phys Chem C* **114**(5): 2256–2266 (2010)
- [52] Bhowmik S, Naik R. Selection of abrasive materials for manufacturing grinding wheels. *Mater Today Proc* **5**(1): 2860–2864 (2018)
- [53] Klaffke D. On the repeatability of friction and wear results and on the influence of humidity in oscillating sliding tests of steel-steel pairings. *Wear* **189**(1–2): 117–121 (1995)
- [54] Oh H K, Yeon K H, Kim H Y. The influence of atmospheric humidity on the friction and wear of carbon steels. *J Mater Process Technol* **95**(1–3): 10–16 (1999)



Solène BARLEMONT. She received her master's degree in mechanical engineering from University of Technology of Compiègne, France,

in 2020. She is performing her Ph.D. degree at Femto-ST Institute, France, since 2020. Her main interests concern the behavior of Bulk Metallic Glasses during tribological solicitations.



Paul LAFFONT. He received his master degree in functional advanced materials and engineering from both Grenoble-INP Phelma, France, and Catholic University of

Louvain, Belgium, in 2020. He is now performing his Ph.D. degree at the SIMaP laboratory, France. His main interests concern the elaboration and thermal treatments of metallic glasses in order to assess the tribological behavior.



Rémi DAUDIN. He received his Ph.D. degree in condensed matter physics from the Grenoble University, France, in 2012, for his studies on the metallic liquid structure at a liquid/solid interface. He continued with a three-year post-doc position at SIMaP laboratory, France, in the field of *in situ* X-ray tomography during

the solidification of metal-matrix nano-composites. After a one-year position at Catholic University of Louvain, Belgium, on metallic glass thin films, he joined the SIMaP laboratory, France, in 2017, where his main interests concern the relationship between the structural state, the deformation mechanisms, and the mechanical properties of metallic glasses.



Alexis LENAIN. He received a Ph.D. degree in metallurgy at the SIMaP laboratory, France, in 2017, focused on learning about the chemistry of metallic glasses. His research focused on developing new alloys combining several functional properties such as low thermal conductivity and good mechanical properties. He also worked alongside with

his Ph.D. director Sebastien GRAVIER to promote the research work carried out so far on the shaping processes to create Vulkam: a deeptech start up in metallurgy. Vulkam's ambition is to promote new highly functional alloys in the industry of watches and medical devices, using its proprietary unique process and its ability to develop specific metallic glasses. He is now in charge of the development of the new range of alloys and the elaboration process.



Guillaume COLAS. He received his Ph.D. degree in tribology from INSA Lyon, France, in 2013, for his work on the tribology of dry lubricants for space applications and the effect of the space environments on friction and wear. He pursued his research with 5 years postdoctoral position, first at INSA Lyon, France (8 months), on the tribology of self-lubricating composite materials for space applications, then at University of Toronto, Canada,

to work on the nanomechanics and nanotribology of MoS₂-based coatings and two-dimensional (2D) materials (graphene, graphene oxides, MoS₂, and WS₂) in controlled environment. He joined Institut FEMTO-ST, France, in 2018, first as a postdoctoral research fellow, then as a CNRS researcher from October 2018. His main interests are the tribology of dry and dry-lubricated contacts as a function of working environments and the micro- and nano-mechanical properties of the resulting interfacial material.



Pierre-Henri CORNUAULT. He received his master degree in mechanical engineering from University of Technology of Compiègne, France, in 2003, his postgraduate degree in Materials Science from University of Lyon, France, in 2004, and obtained his Ph.D. degree in

tribology from Ecole Centrale de Lyon, France, in 2008. He is currently an associate professor in Materials Science at the University of Bourgogne Franche-Comté, France. His research focuses on the tribological behavior of dry contacts with a special interest in the dynamics of the interface renewal and the characterization of surface modifications during friction.